Borges, M.F.; Amancio-Filho, S.T.; dos Santos, J.F.; Strohaecker, T.R.:
Development of computational models to predict the mechanical behavior of Friction Riveting joints
In: Computational Materials Science (2011) Elsevier

DOI: 10.1016/j.commatsci.2011.10.031

Development of computational models to predict the mechanical behavior of Friction Riveting joints

M.F. Borges [a,b], S.T. Amancio-Filho [c, d], J.F. dos Santos [c], T.R. Strohaecker [a], J.A.E. Mazzaferro [b]

[a] *Universidade Federal do Rio Grande do Sul / PPGEM-DEMET / LAMEF, Av. Bento Gonçalves 9500, setor IV, prédio 75, sala 205, Porto Alegre, Rio Grande do Sul, Brazil.*
[b] *Universidade Federal do Rio Grande do Sul / PROMEC-DEMEC, Rua Sarmento Leite, nº 425, Bairro Cidade Baixa Porto Alegre – RS, Cep 90050-170 Porto Alegre, Rio Grande do Sul, Brazil.*
[c] *Helmholtz-Zentrum Geesthacht / Institute of Materials Research – Materials Mechanics, Solid State Joining Processes (WMP) and Advanced Polymer-Metal Hybrid Structures Group, Max-Planck-Str. 1, D21502, Geesthacht, Germany.*
[d] *Corresponding author: Tel.: +49 4152 87 2066; Fax: +49 4152 87 2033; Email: sergio.amancio@hzg.de*

Abstract

Friction Riveting (FricRiveting) is a new, friction based, spot joining process for polymer-metal hybrid structures that has been studied experimentally in recent years. The process provides a cost effective and fast alternative to conventional joining methods, such as riveting and adhesive bonding. In this work, finite element analysis was performed to predict the behavior of overlap and point-on-plate FricRiveting joints with the objective of supporting the further development of the process. Additionally, it is intended to provide a better understanding of the mechanical behavior of the joint. The analyses were performed by simulating joints made of polyetherimide extruded plaques and high-strength aluminum alloy AA2024-T351 rivets using an FEA package. Model validation was carried out with three different types of mechanical tests: tensile, lap shear and T-pull. The results obtained in this preliminary work were most encouraging since the developed models were able to predict experimental behavior with accuracy.

Keywords: Friction Riveting; hybrid joints; Polymer-Metal; FEA; mechanical fastening.

1. Introduction

The global pressure to reduce emissions, combined with a constant increase in fuel prices in recent years, has culminated in a need for new lightweight materials, such as engineering plastics. This is attributed to the fact that the use of metallic structures alone cannot satisfy these needs. Targeting these new objectives, the transportation industry initiated research into new processes to produce lightweight materials with elevated weight-strength ratios [1]. New structures composed of two or more different materials are now often found in industrial products. These new multi-material hybrid constructions are becoming more common and, at the same time, more complex [2]. For this reason, there is a need to develop new fabrication processes to produce and assemble these structures.

One of the new multi-material concepts is metal-polymer hybrid structures. The presence of connections is a common design feature in these structures. It is well known that metals and polymers have a limited joinability by conventional joining methods such as welding [3]. Among the major difficulties in joining these materials are the significant physical-chemical dissimilarities between them and different thermal expansion coefficients, which can induce a gradual loss of strength in the joint. For this reason, the most common joining methods for polymer-metal hybrid joints are mechanical fastening and adhesive bonding [3]. These techniques have several limitations. These include long curing times, short shelf-life and disposal issues in the case of adhesive bonding and, in the case of mechanical fastening, increased local stress around the fastener through-hole located in the joining pieces caused by fastener load transfer. The new FricRiveting process was developed and patented by Helmholtz-Zentrum Geesthacht to mitigate these limitations [4]. It provides joints with improved mechanical properties that

can be produced within short time-frames [5]. Furthermore, the joint surfaces need only minimal preparation, which makes the process more efficient and environmentally friendly [6]. The potential of the technique has attracted the attention of the European Transportation Industry and of the international community and was awarded several R&D prizes, such as the Granjon Prize 2009[1] of the International Institute of Welding. Currently different R&D industrial partners[2] such as Airbus Deutschland, are investigating the feasibility of the technique in their structural polymer-metal parts.

The principles of FricRiveting are illustrated in Figure 1. In the basic process configuration, a high-speed rotating pin (the rivet) is pressed against a fixed thermoplastic part (**Figures 1A and 1B)**. Local frictional heat melts the polymeric material, forming a molten layer around the rivet (**Figure 1B**). At the end of the heating phase, the tip of the rivet becomes plasticized (softened) due to the local increase in temperature. The plasticized rivet tip begins to deform, as the forging force (an increase in the axial force) is applied (**Figure 1C**). After a short cooling interval the joint consolidates. The final geometry of the rivet is a parabolic anchor inside of the polymeric base plate with approximately twice the initial rivet diameter (**Figure 1D**).

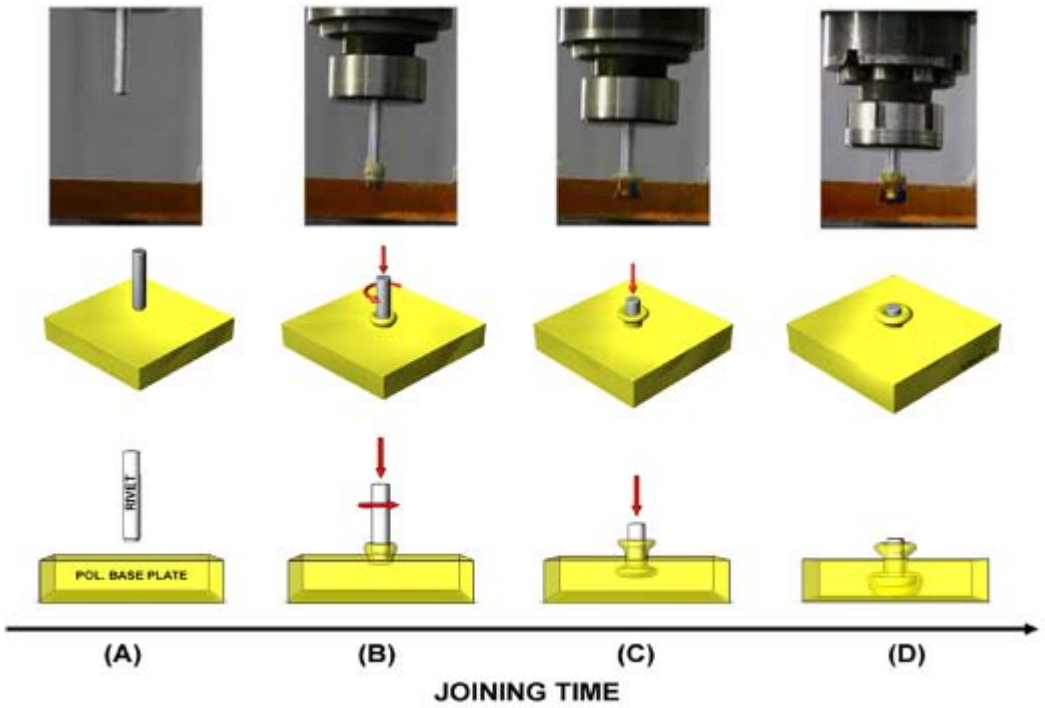

Figure 1 – FricRiveting process scheme. (A) Positioning and clamping of joining partners, (B) Insertion of rotating rivet into the base plate, (C) Rotation braking and rivet forging, (D) Cooling and consolidation. Adapted from reference [6].

Due to the growing popularity of polymer-metal structures observed in recent years, two potential fields of application of this new joining process are to be found in the automotive and aerospace industries. However, before implementating this new process in the production environment, the mechanical performance of FricRiveting must be further investigated. This investigation is fundamental for the design and fabrication of high damage-tolerance products. Currently, an important tool to optimize processes and geometries, leading to time and costs savings, is the elaboration of finite element models (FEM) by CAE software. When calibrated and validated by experimental testing and material

[1] http://www.iiwelding.org/TheIIW/Recognition/Pages/Granjon.aspx , 8th Feb. 2011

[2] Evaluation of feasibility of FricRiveting in aeronautical composite-titanium structures, Cooperation Project between HZG-Airbus Deutschland, 2009-2012

characterization data, FEM models can strongly contribute to the understanding of mechanical behavior and bonding mechanisms of FricRiveting joints, enabling the new process and joint performance to be improved.

In the case of FricRiveting, no previous modeling studies have been published. For this reason, different FEM models have to be developed and tested, initially to allow the selection of the best approach describing the materials behavior. As a second step, a final joint geometry model has to be defined and validated by mechanical testing data to finally generate a trustworthy model.

The aim of this work was therefore to develop an FEM computer-based model capable of predicting the static mechanical behavior of FricRiveting joints. Different finite elements models of base materials and joint geometries were investigated using commercial FEA software (ABAQUS).

2. Material and Methods

2.1. Base Materials

2.1.1. AA2024-T351 Extruded Rods

Extruded rods of aluminum AA2024-T351, a high-strength Al-Cu-Mg alloy [7], with diameters of 10 mm were used to machine rivets with diameters of 5 mm and lengths of 50 mm (for the lap shear specimens) and 60 mm (for the T-Pull tensile testing specimens) [8]. The mechanical properties of this alloy are presented in **Table 1**. Average Vickers microhardness (HV) measurements are additionally given in this table.

Table 1 - Mechanical properties of the AA2024-T351 aluminum alloy [7, 9].

Yield strength, σ_v [MPa]	Ultimate Strength, σ_u [MPa]	Elastic Modulus, E [GPa]	Poisson's Ratio	Microhardness [HV]
327	451	73.1	0.33	141.5 ± 6.6

2.1.2. Polyetherimide (PEI)

Polymeric base plates for FricRiveting were produced from extruded 13.4 mm polyetherimide PEI plaques (GE Plastics ULTEM-1000) [10]. PEI is an amorphous high-performance engineering thermoplastic, characterized by high strength and rigidity at room and elevated temperature, good long-term stability and excellent dimensional stability. The mechanical properties of PEI in the extrusion direction are presented in **Table 2**, with the experimental average Vickers microhardness results for the investigated plaques.

Table 2 - Mechanical properties of the ULTEM-1000 used in this work [5].

Yield strength, σ_v [MPa]	Ultimate Strength, σ_u [MPa]	Elastic Modulus, E [GPa]	Poisson's Ratio	Microhardness [MPa]
69	120	2.88	0.39	284

2.2. FricRiveting Joints

A commercial friction welding machine (RMS 200, Harms & Wende, Germany) was used to produce the FricRiveting joints used in this study. Parameter optimization based on previous work [5] was carried out, and the following process parameters were selected to produce the joints for this study: axial pressure of 7 bar, rotational speed of 21,000 rpm and joining time of 3 s. These parameters are responsible for the frictional heat generation and material plasticization. After the forging phase, the deformed tip of the rivet forms the anchoring zone (AZ) in the polymeric base plate, as illustrated in **Figure 2A**, which has been demonstrated to be the strongest part of the joint [11]. Amancio [5] determined the differences in mechanical behavior within this region, based on microhardness testing and

thermal analyses. The author [5] subdivided the rivet and the polymeric base plate into Base Material (BM), Heat Affected Zone (HAZ) for thermally treated regions and Thermo-Mechanical Affected Zone (TMAZ) for the regions with microstructural modifications as a consequence of concomitant mechanical and thermal processing. Typical microstructural zones and a microhardness map of a FricRiveting joint are shown in **Figure 2A** and **Figure 2B**.

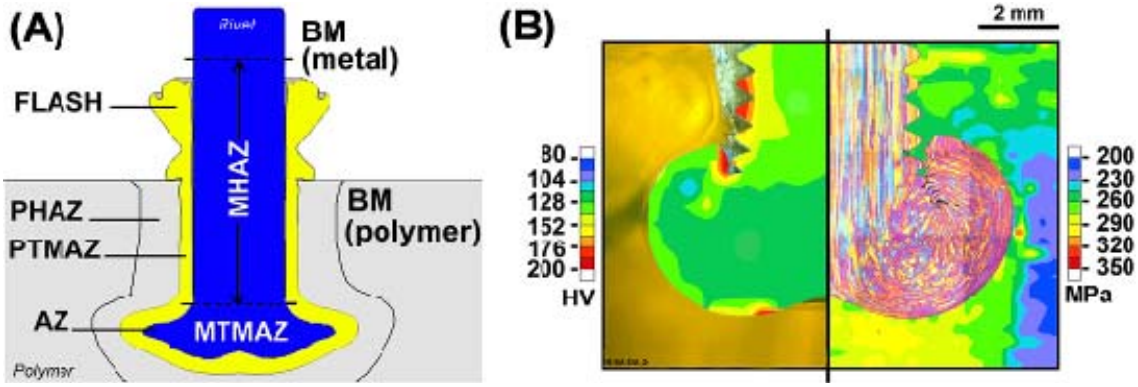

Figure 2 – (A) Microstructural zones of a typical friction riveted joint: MHAZ Metal Heat Affected Zone, MTMAZ Metal Thermo-Mechanically Affected Zone, PHAZ Polymer Heat Affected Zone, PTMAZ Polymer Thermo-Mechanically Affected Zone and BM Base Material, (B) Schematic superposition of the microstructure and microhardness distribution of a typical AA 2024-T351 / PEI FricRiveting joint: on the left is the aluminum alloy hardness map (1-MHAZ, 2-MTMAZ) and the PEI microstructure, on the right the microhardness distribution of PEI (3-PTMAZ) and the microstructure of the aluminum alloy. Adapted from reference [5].

The joint mechanical behavior can be estimated from the microhardness as demonstrated by Mazzaferro et al. [12] in their simulation studies on Friction Spot Welding of aluminum alloys due to the well-known Tabor's relation, in which microhardness is directly proportional to bulk properties [13]. This approach has been used due to the inherent difficulties in determining experimentally the local properties of the individual microstructural zones. **Table 3** shows the multiplication factors used to simulate the mechanical properties of joint based on the microhardness of the microstructural regions modeled in this work.

Table 3 - Multiplication factors used in this work to represent the mechanical properties of the microstructural zones in friction riveted joints

Material	Base Material (BM)	HAZ	TMAZ
AA2024-T351	1	0.95 of BM	0.85 of BM
PEI ULTEM-1000	1	1.1 of BM	0.9 of BM

2.2.1. Mechanical Testing

2.2.1.1. Tensile Testing of Base Materials and Lap Shear Testing of Riveted Joints

Tensile testing of base materials was performed with flat specimens in accordance with DIN 53455 [14] (**Figure 3A**). The selected lap shear specimen geometry was in agreement with ASTM-D5961/D5961M-05 [15], as shown in **Figure 3B**. Two plaques of PEI with dimensions 189 x 36 x 5 mm were single-riveted with an overlap of 36 mm by an AA2024-T351 aluminum rivet with a diameter of 5 mm. The exposed length of the rivet was set to 20 mm. Mechanical testing was carried out in a Zwick/Roell 1478 servo-electric test machine equipped with a 10 kN load cell. The testing transverse speed was 2 mm/min at room temperature (21°C).

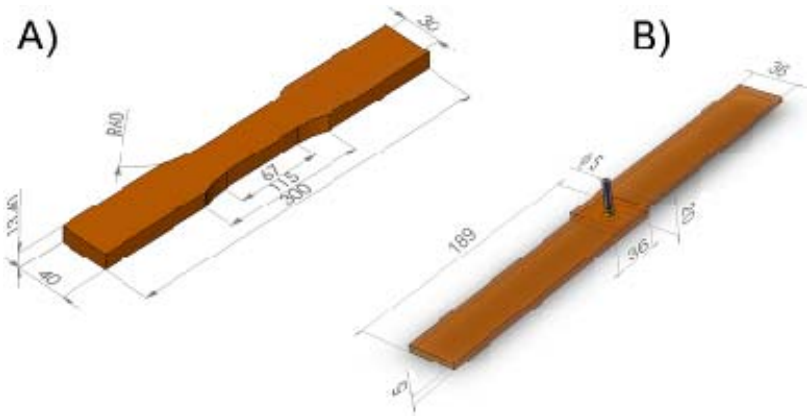

Figure 3 – (A) Flat tensile specimen geometry, (B) Geometry of single-riveted lap shear joints.

2.2.2. T-Pull Tensile Testing

The point-on-plate joint configuration used for T-pull tensile testing is presented in **Figure 4A**. It consists of a modified geometry with a base plate of PEI with 70 x 70 x 13.4 mm [5] and a metallic rivet with diameter of 5 mm and 60 mm long (geometry based on DIN EN ISO 898 [16]). T-pull tensile tests were performed in an INSTRON 1195 testing machine, equipped with a 50 kN load cell and a tailored specimen holder (**Figure 4B**). Testing traverse speed was 1 mm/min at room temperature (21°C).

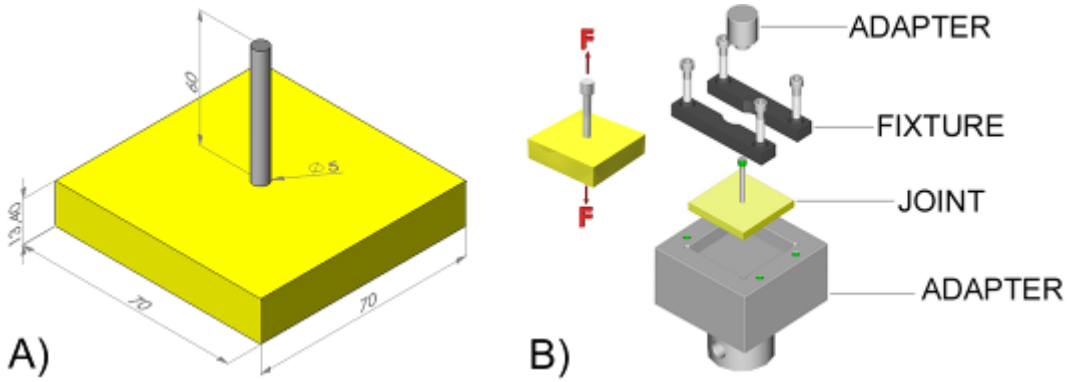

Figure 4 – (A) T-pull tensile specimen geometry, (B) Schematic representation of the T-pull tensile testing jig used for the evaluation of the tensile properties in FricRiveting point-on-plate joints.

2.3. Finite Element Method

All models and simulation results presented in this work were obtained with Abaqus 6.8-1 CAE software [17]. For the validation of base material models, flat tensile specimens (see Section 2.3.1) were selected, while the mechanical behavior under static condition of friction riveted joints was modeled by both lap shear and T-pull tensile testing (see Section 2.3.2).

2.3.1 Base Material FE Models

It is well known that materials will undergo extensive plastic deformation during the lap shear and T-pull tensile tests of FricRiveting joints [18]. Under these testing conditions, most materials behave in a non-linear manner. Therefore, the proposed base materials models are assumed to behave according to non-linear modes. The meshing applied in all base material models is composed of hexahedrical eight-node (Abaqus C4D20R) mesh elements. For the PEI material model, four different

models were tested: Viscoelastic, Elastic-Plastic, Elastic-Plastic with Johnson-Cook failure description and Hyperelastic. Because this polymer has a viscoelastic mechanical behavior [19] with strain rate and temperature dependence, all models tested were only approximations. It is important to mention that the input material properties used in this work were kept constant for all material models investigated.

Considering that aluminum 2024-T351 has well-established mechanical behavior [20, 21], only one model, i.e., the classical Elastic-Plastic mechanical behavior model, was built in the FEM simulation. This model describes this alloy very well, as previously shown by Fersini and Pirondi [9] in fracture-simulation models of overlap spot welds. The material's input values and model constants were added as described in this section. Additionally, the Johnson-Cook criterion with isotropic hardening fracture model (J-C) [22, 23] was evaluated for the aluminum attempting to simulated the final failure of the mechanical testing specimens. The J-C fracture model presents a component for the material model formulation (**Equation 1**) associated with a shear failure component (**Equation 2**), which corresponds to the damage initiation criterion [23].

$$\bar{\sigma} = \underbrace{\left(A + B\bar{\varepsilon}^{n}\right)}_{\substack{Elasto-Plastic \\ term}} \underbrace{\left[1 + C\ln\left(\frac{\dot{\bar{\varepsilon}}}{\dot{\bar{\varepsilon}}_0}\right)\right]}_{\substack{Viscosity \\ term}} \underbrace{\left[1 - \left(\frac{T - T_{room}}{T_{melt} - T_{room}}\right)^{m}\right]}_{\substack{Softening \\ term}} \quad (1)$$

$$\bar{\varepsilon}_{oi} = \left[D_1 + D_2 \exp\left(D_3 \frac{P}{\bar{\sigma}}\right)\right] \times \left[1 + D_4 \ln\left(\frac{\dot{\bar{\varepsilon}}}{\dot{\bar{\varepsilon}}_0}\right)\right] \left[1 + D_5\left(\frac{T - T_{room}}{T_{melt} - T_{room}}\right)\right] \quad (2)$$

where $\bar{\sigma}$ is the equivalent plastic flow stress, $\bar{\varepsilon}$ is the equivalent plastic strain, $\dot{\bar{\varepsilon}}$ is the plastic strain rate, $\dot{\bar{\varepsilon}}_0$ is the reference strain rate (1.0 s^{-1}) and $\bar{\varepsilon}_{oi}$ is the plastic strain at damage initiation. According to Johnson and Cook [22, 23], fracture takes place when the the Scalar Damage Parameter (ω) is higher than one. The Scalar Damage Parameter can be described through a cumulative law [24] defined as

$$\omega = \frac{\sum \Delta\bar{\varepsilon}}{\bar{\varepsilon}_{oi}} \quad (3)$$

The adopted J-C material constants were selected from [25] and are given in **Table 4**. The J-C model represents an empirical relationship for the von Mises flow stress [26].

Table 4 - Johnson-Cook parameter values utilized in this work for the aluminum AA2024-T351 alloy [27].

A [MPa]	B [MPa]	n	C	m	D1	D2	D3	D4	D5
352	440	0.42	0.0083	1	0.13	0.13	-1.5	0.011	0

2.3.2. Lap Shear and T-Pull Tensile Test Models

Six volumetric regions (BM-metal, BM-polymer, MHAZ, PHAZ, MTMAZ and PTMAZ, see **Figure 5A**) were created to model the mechanical behavior of the different microstructural zones found in a typical friction riveted joint. The same approach as used by Mazzaferro et al. [15] was adopted. In this approach, FEM models developed, validated and optimized for base materials, are built into the modeled

testing specimens. An important factor controlling the performance of FEM models under static loading arises from the contact points between the different microstructural regions. The way the different objects interact with each other in a simulation is closely related to their contact points [28]. In this manner, contact points should be carefully established, to avoid mutual penetration and deviation in prediction.

The contact properties utilized in this work are shown in **Table 5**. Friction coefficient values ranging from 0.3 to 0.5 were used to calibrate and find the best fitting of the tested models. Supplementary contact points were established for the anchoring zone (AZ), to refine the model accuracy in view of its complex geometry and large degree of deformation during loading.

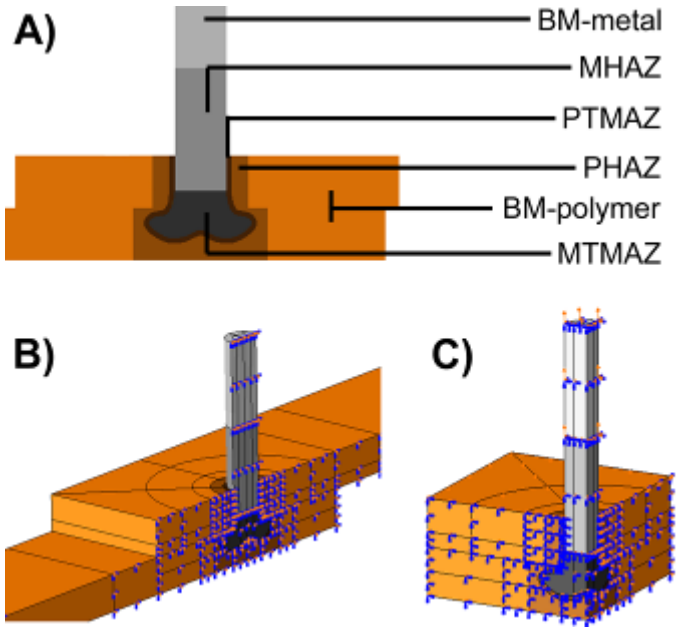

Figure 5 – (A) Interaction between different material volumes, representing the properties of different microstructures in a lap shear testing CAD geometry. Symmetry approach adopted to reduce computing time, (B) Overlap joints (lap shear specimens), and (C) Point-on-plate joints (T-pull tensile specimens).

Table 5 - Contact Proprieties between AA 2024-T351 / PEI for the FEM models.

Normal	**Tangential**	**Friction Coefficient**	**Shear Limit [MPa]**
Hard Contact	Penalty Formulation	0.3-0.5	109

Symmetric models were designed to reduce the calculation time according to the geometrical, boundary conditions and load applied. For the overlap joints, a half-symmetry model (z axis) was adopted, while for the point-on-plate joints a quarter-symmetry model (x and z axis), as respectively shown in **Figures 5B and 5C**. The use of geometrical symmetry additionally helps to prevent errors caused by the presence of asymmetrical mesh elements.

Meshes applied in the testing specimens were generated from tetrahedral elements of quadratic order (Abaqus element type C3D20R), **Figure 6**. The size of the mesh element was changed according to the relevance of deformation mechanisms of the region in the model geometry. Based on this criterion, the interface AA 2024-T351 / PEI, which experiences large strain levels, was modeled with finer mesh elements, intended to reduce noise in the simulated results. Loading and restrictions were applied in the same way to simulate real testing conditions.

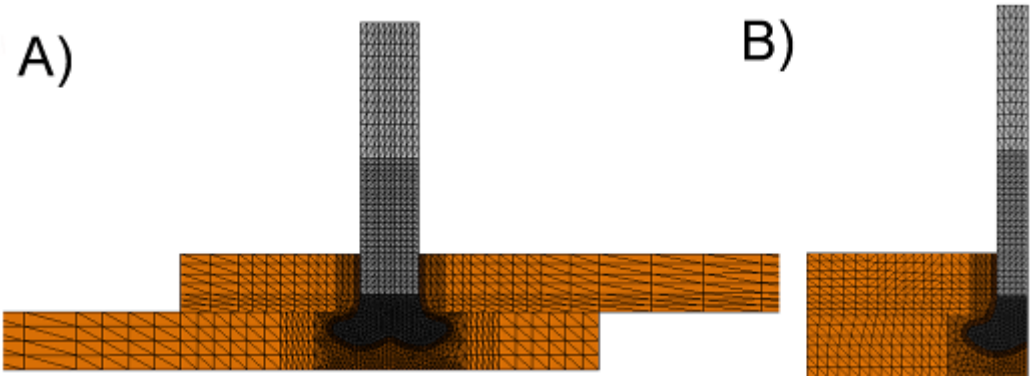

Figure 6 – Mesh elements used in FricRiveting joint FEM models: (A) Overlap (lap shear specimens), and (B) Point-on-plate joints (T-pull tensile specimens).

3. Results and Discussions

The presentation of results is divided into two groups. Firstly, the simulation results of base material are presented and discussed. Secondly, the results for FricRiveting joints and validation of models, based on experimental mechanical testing, are addressed.

3.1. FEM Modeling

3.1.1. Aluminum AA2024-T351

The aluminum alloy used in this work can be considered an incompressible material because of its classical elastic-plastic (E-P) behavior. The AA2024-T351 alloy was modeled by using E-P and a hybrid E-P/J-C model (from Abaqus' built in subroutines) containing a fracture model for isotropic hardening. The E-P/J-C model was investigated for the aluminum alloy because final failure can occur in the metallic rivet, such as in the case of T-pull tensile specimens. **Figure 7** presents the simulated and experimental results for tensile testing in the AA2024-T351 base material. The simulated results agreed well with a typical elastic-plastic material as observed by Fersi and Pirondi [9], fitting the experimental curve with an acceptable error level (**Figure 7A**). Some deviations were present in the modeled stress-strain curves. The sharp transition between the elastic and plastic regions in the stress-strain curves of the investigated E-P and E-P/J-C models is probably associated with a software calculation, which is closely related to the available input variables. Such deviations can occur because most commercially available FEM software, including Abaqus, uses only a few input parameters to describe the material's mechanical properties. The fracture prediction curve based on J-C criteria is also shown in **Figure 7A**. Final failure can be identified at the point where the E-P coupled J-C criterion curve suddenly decreases at the end of the plastic deformation regime.

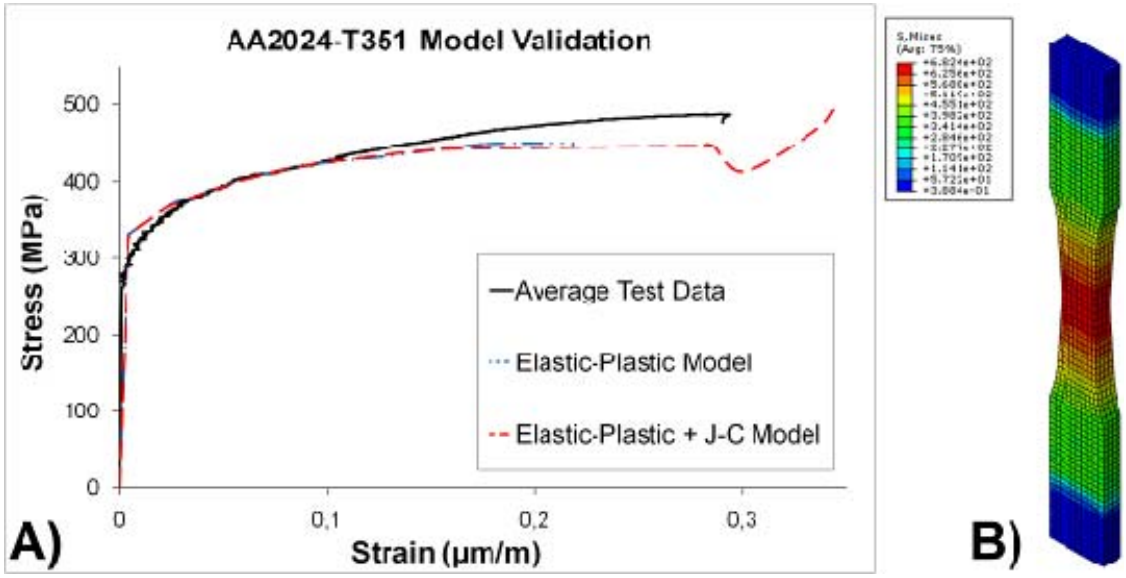

Figure 7 – FEM simulation and experimental results (average of 3 specimens) for the tensile behavior of AA2024-T351 base material. (A) Stress –strain curves, (B) Von Mises stress distribution under tensile loading.

3.1.2. FEM Modeling of PEI

PEI is a very brittle engineering plastic, exhibiting a stress-strain curve similar to aluminum. From the current knowledge of the authors, there are no models for the PEI base material available in the literature for comparison. For this reason, the E-P and Hyperelastic models (chosen from the Abaqus built in subroutines) were applied for modeling the mechanical behavior of the PEI polymer. These two models do not take into account the viscoelastic (chain relaxation) component typical of plastics under mechanical load. Nevertheless, they were able to provide curves indicating a good fitting accuracy with the experimental data up to the point at which ultimate tensile strength is achieved, as observed in **Figure 8A**. After achieving maximum stress both curves tend to lose precision and begin deviating from experimental tensile testing results. Although these models presented the above mentioned limitations, computing time is short, without resulting in any significant deviation from the true tensile properties. Further simulation work is required, tackling different strain and temperature ranges to decrease the identified limitations.

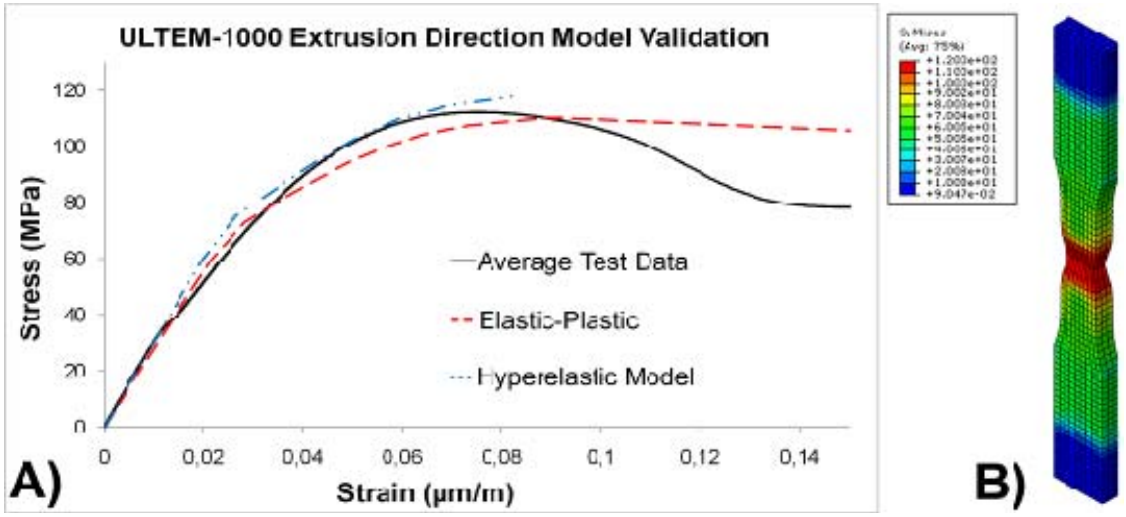

Figure 8 – FEM simulation and experimental results (average of 3 specimens) for the tensile behavior of the PEI base material. (A) Stress –strain curves, (B) Von Mises strain distribution under tensile loading.

3.1.3. Lap Shear Testing

Lap shear tests (three replicates) were performed to validate the respective models. Initially, the static efficiency, the maximum load and the load displacement behavior were evaluated. These results were used to compare and validate the numerical models and finally select the model with highest accuracy. Models were tested by applying different contact conditions to minimize possible discrepancies associated with the selection of the local material properties input data.

Five control parameters were selected for the direct comparison between model and experimental data:

- Plate displacement – Displacement in Y axis;
- Plate separation – Displacement in X axis;
- Pin rotation angle – Rotational displacement in Z axis;
- Maximum Load – Max. tensile force;
- Critical Load – Load for complete separation of the plates.

Three displacement stages (at 1.2 mm, 3.1 mm and 6.3 mm) from the lap shear testing were selected for evaluating the accuracy of the modeled results. An example of the evolution of the model to the real experiments can be seen in **Figure 9**. In the first stage (**Figure 9A**) secondary bending is initiated and the overlap area is slightly rotated from its initial plan parallel to the direction of lap shear loading. In the second stage (**Figure 9B**) increasingly secondary bending induces the separation of the upper and lower polymeric pieces. Finally (stage 3, **Figure 9C**) severe plastic deformation in the polymeric volume around the rivet causes the upper polymeric piece to start slipping over the rivet shaft; at this stage the joint looses its structural integrity. It is possible to observe good agreement between the controlling parameters of the modeled diagrams and the experimental snapshots taken during testing.

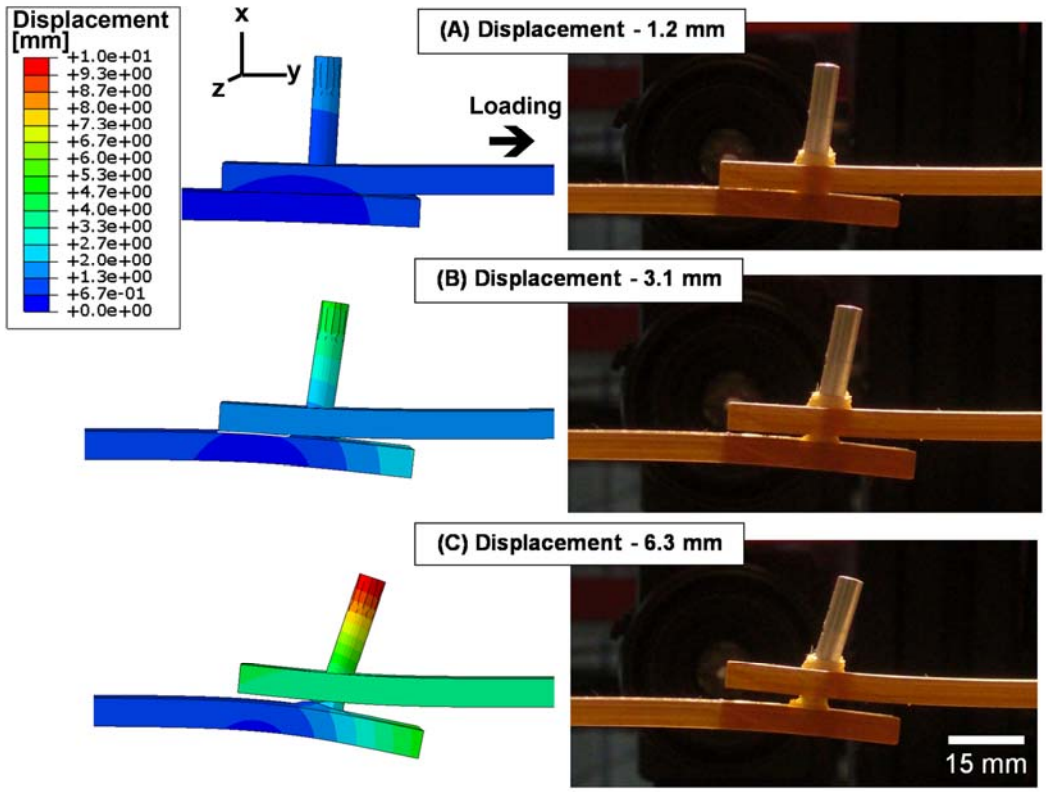

Figure 9 – Comparison between modeled and experimental lap shear testing of a friction riveted join; on the left of the figure, the simulation results for the displacement in the y-axis direction, on the right, snapshots during testing, shown for the same displacement stages: (A) 1.2 mm (B) 3.1 mm (C) 6.3mm.

Figure 10 shows the predicted and experimental results for the lap shear testing. The output simulation results for the overlap joints (lap shear tests) showed comparable behavior to the modeled base materials (compare **Figures 7A, 8A and 10A**). The E-P modeled joint mechanical behavior resulted in good convergence and shorter computational times (**Figure 10A**). When the proposed Hyperelastic model was used, the results indicated less convergence and longer computational times.

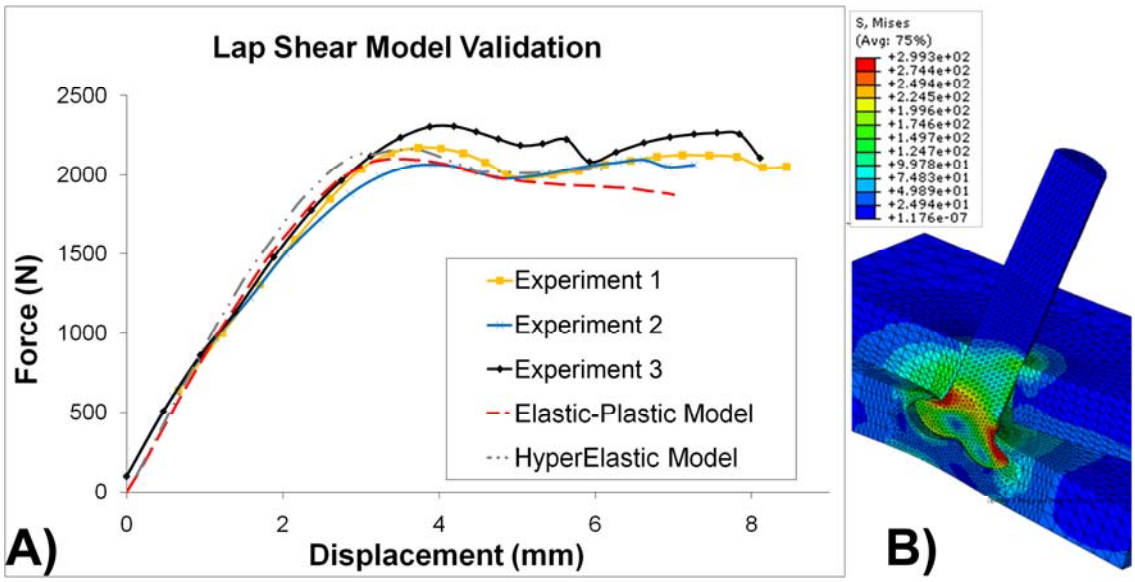

Figure 10 – Experimental and modeled lap shear testing results. (A) Force versus displacement curves, and (B) Finite Element Analyses showing the stress distribution of a modeled joint.

The displacement behavior of the modeled curves presented an average deviation of about 10% in comparison with the experimental results (see **Figure 10A**), which is an acceptable error, considering the geometric complexity of the FEM models and the complex failure mechanisms found in FricRiveting joints. The source of this deviation is assumed to be mainly associated with the simplifications used to describe the mechanical behavior of the polymeric material (absence of the viscoelastic component), eventual losing of contact points due to the complex contact boundary conditions and the interaction between the dissimilar base materials. For all investigated contact conditions, the best results were achieved when a dry friction coefficient of 0.39 was applied for the PEI-PEI and 0.37 for aluminum-PEI interfaces.

In friction riveted overlap joints, structural failure is assumed to happen when the complete detachment of the upper and lower plaques takes place and the upper and lower plaques start to slide along the rivet shaft [5]. Consequently, the proposed models lose precision and the joint strength decreases after complete plate detachment occurs because the slide along the pin is not a quasi-static process. The sliding action of the plaques begins at about 5 mm of test displacement after complete detachment and is seen as oscillations in the experimental stress-displacements curves (see **Figure 10A**).

3.1.3. T-Pull Tensile Testing

The results of T-pull tensile testing predicted in this work also showed similar features in comparison with the proposed base material models. **Figure 11** illustrates the simulated and experimental curves for T-pull tensile testing of point-on-plate joints. Similar to observations in the lap shear testing, the modeling of the point-on-plate joints presented fairly good convergence and a shorter computational time. However, current T-pull tensile FE models were not able to completely fit the experimental curve (see **Figure 11A**). This larger deviation error, when compared with the lap shear testing models, is probably associated with geometrical simplifications and the virtual hindering locations (fixing sites) of the modeled testing specimen.

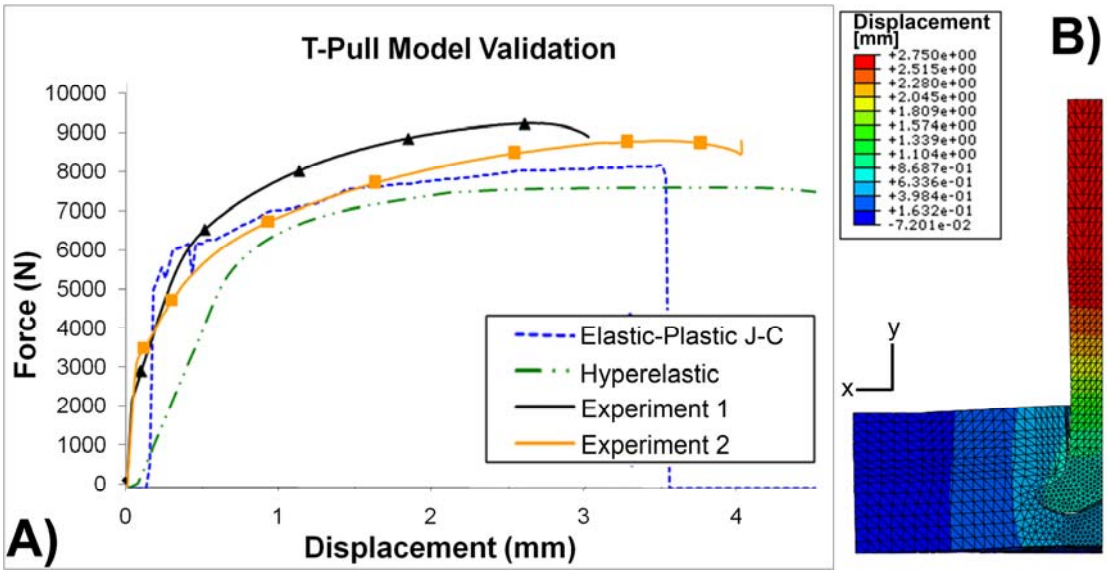

Figure 11 – Experimental and modeled T-pull tensile testing results. (A) Force versus displacement curves, and (B) Finite Element Analyses showing the displacement distribution in the y-axis for the modeled joint.

Optimized FricRiveting joints on non-threaded AA 2024-T351 / PEI will always fail outside the joint area, in the metallic rivet shaft [11]. Keeping this in mind, the Johnson-Cook failure model was added to the modeled T-pull tensile specimens. In this way, the proposed model is able to provide the exact location and moment of the final failure, which will take place when the J-C damage parameter reaches one (and the test force goes to zero, see **Figure 11A**). The accuracy of the J-C model can be further observed in **Figure 12A**, where two final stages of a FEM simulation for a T-pull tensile specimen are exemplified. **Figure 12B** presents the appearance of a T-pull tensile specimen prior to (**Figure 12A-1**) and after testing (fractured rivet, **Figures 12A-2 and 12A-3**). The stress concentrates in the rivet's body in regions outside of the polymeric plate, prior to crack initiation (**Figure 12A-1**). The location of the final failure in the modeled specimen also exhibits a high level of agreement with tested specimens (compare **Figure 12A-2 with Figure 12B-2 and Figure 12B-3**). A similar approach for an investigation into the controlling parameters at different stages of the T-pull tensile testing is in progress and will be discussed in future publications.

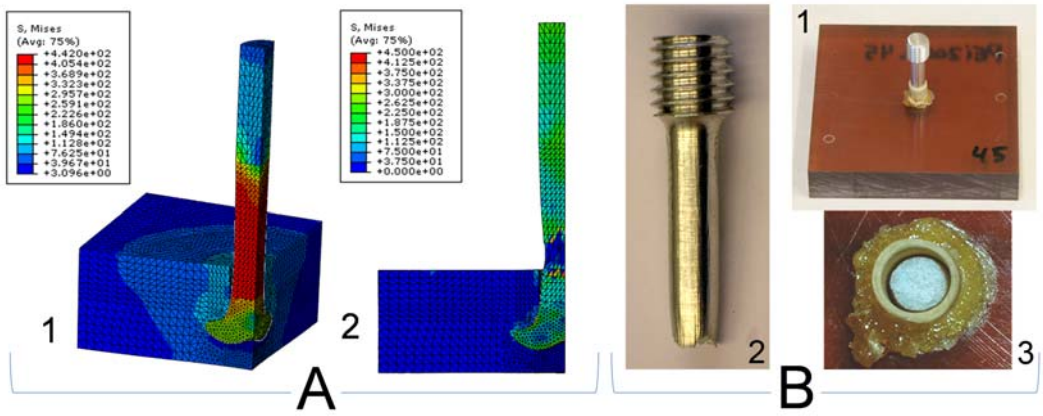

Figure 12 – Failure mechanisms of modeled and experimentally tested T-pull tensile specimens. (A) Position 1 shows the stress concentration prior to failure and position 2 the final failure in the outer rivet shaft, (B) Experimental T-pull tensile specimen: Position 1 shows the joint prior to testing, position 2 shows the crack position in the metallic rivet and position 3 displays the top view of the remaining rivet portion left behind in the polymeric base plate, respectively.

4. Conclusions and Final Remarks

The results obtained in the present work indicate that it is possible to apply FEM analysis to simulate the mechanical behavior of FricRiveting joints tested under monotonic loading. The two different material models (Elastic-Plastic and Hyperelastic) tested for the base materials presented fairly good results. In the case of the polymeric base material, further improvement on model accuracy may be achieved by selecting and investigating alternative mathematical models, such as those assuming viscoelastic properties. However, an increase in calculation time is expected as a result of the required use of the additional heavy CAE subroutines normally associated with those models.

The proposed preliminary FE models for the lap shear and T-pull tensile testing showed an average deviation of about 10% in comparison with the experimental data. The current margin of error allows these preliminary models to be used as a tool for process optimization. These models can be used, for instance, in the development of improved rivet geometries and further help with understanding the effect of processing on joint formation and performance. Moreover, important reference input values could be generated, such as an adequate material friction coefficient between AA 2024-T351 / PEI, self contacts and contact distributions. These could be used in the development of improved FE models as well as providing a starting point for the simulation of different joint geometries, potentially leading to cost savings related to a reduction in the amount of experimental work required.

5. Acknowledgements

The authors would like to acknowledge the financial support given by the Helmholtz Association, Germany within the scope of the grant issued for the Helmholtz-University Young Investigator Group “Advanced Polymer-Metal Hybrid Structures”.

6. References

[1] J.L. Hecht, Macrocomposites made by injection molding, Polymer Composites, 7 (3) (1986), pp 186-190.
[2] A. Mavel, APME, A material choice for the automotive industry, insight into consumption and recovery in Western Europe, Brussels, 1999.
[3] S.T. Amancio-Filho, J.F. dos Santos, Joining of Polymers and Polymer–Metal Hybrid Structures: Recent Developments and Trends, Polym. Eng. Sci., 49 (8) (2009), 1461-1476.
[4] S.T. Amancio-Filho et al., DE 10 2005 056 606 A1: Verfahren zum Verbinden eines metallischen Bolzens mit einem Kunststoff-Werkstuck, German Patent Office, 2005.
[5] S. T. Amancio-Filho, Friction Riveting: development and analysis of a new joining technique for polymer-metal multi-materials structures, Welding in the World, 55 (01-02) (2011), 13-24.
[6] S. Amancio-Filho, J.F. dos Santos. FricRiveting: A new technique for joining thermoplastics to lightweight alloys, in Proc.: Annual Technical Conference of the Society of Plastics Engineers - ANTEC 2008 (2008) pp- 841-845, Milwaukee, USA.
[7] ASM Handbook of Aluminum and aluminum alloys, 3rd ed., ASM International, USA, 1996.
[8] S.T. Amancio-Filho, J.F. dos Santos, Entwicklung des Reibnietens als neues Fügenverfahren für Kunststoff und Leichtbaulegierungen, Materialwissenschaft und Werkstofftechnik, 39 (11-12), 799-805.
[9] D. Fersini, A. Pirondi, Analysis and Modeling of fatigue failure of friction stir welded aluminum alloy single lap joints, Engineering Fracture Mechanics 75 (2008) 790-803.
[10] ASM, Engineering Plastics 1st ed. Engineered Materials Handbook Vol. 2, ASM International, 1998.
[11] S.T. Amancio, J.F. dos Santos, V. Ventzke, Determination of fracture mechanisms under tensile loading in a commercially available engineering thermoplastic material joined by FricRiveting, Proceedings of the 5th International Conference on Fracture of Polymers, Composites and Adhesives, 7-11 September 2008.
[12] J.A. Mazzaferro, T.R. Strohaecker, J.F. dos Santos, T.S. Rosendo, C.C. Mazzaferro, F.D. Ramos, M.D. Tier, Preliminary Study on the Mechanical Behavior of Friction Spot Welds, IIW, São Paulo, 2008.

[13] D. Tabor, The hardness of metals, Oxford University Press, New York, 1951.
[14] DIN 53455, Prufung von Kunststoffen, Zugversuch. DIN – Deutsches Institute fur Normung e. V., 1981.
[15] ASTM-D5961/D5961M-05, Standard test method for bearing response of polymer matrix composite laminates, ASTM International, USA, 2005.
[16] DIN EN ISO 898-1, Mechanische Eingenschaftten von Verbindungselementen aus Kohlenstoffstahl und legierten Stahl – Teil 1: Schrauben. DIN – Deutscher Institut fur Normung e. V., 1999.
[17] Abaqus v. 6.8-1 Documentation, under license for Helmholtz-Zentrum Geesthacht (formerly GKSS Forschungszentrum Geesthacht GmbH), Germany, 2010-2011.
[18] S.T. Amancio, J.F. dos Santos, Rebitagem por Fricção ("FricRiveting"): Desenvolvimento de uma nova técnica de união para juntas híbridas do tipo polímero-metal, XXXV Consolda, ABS, Piracicaba 2009.
[19] G. Zhan, Y. Yu, et al, Further Study of Viscoelastic Phase Separation of Cyanate Ester Modified with Poly(etherimide), Journal of Polymer Science, part B, Vol 44 (2006), 517-523.
[20] DOT/FAA/AR-03/57, Failure Modeling of Titanium 6AL-4V and Aluminum 2024-T3 with the Johnson-Cook Material Model, U. S. Federal Aviation Administration (FAA), Final Report September 2003.
[21] G. Borino, P. Fuschi and C. Polizzotto**,** Elastic-Plastic-Damage Constitutive Models with Coupling Internal Variables, Mechanics Research Communications Volume 23, Issue 1, January-February (1996), 19-28.
[22] V.J. Lemaitre, R. Desmorat, Engineering Damage Mechanics: Ductile, Creep, Fatigue and Brittle Failures, Springer, 1 edition, Berlin, 2005.
[23] G.R. Johnson, W.H. Cook, Fracture characteristics of three metals subjected to various strains, strains rates, temperatures and pressures, Engineering Fracture Mechanics 21/1 (1985) 31-48, 1985.
[24] S. Dey, T. Borvik, O.S. Hopperstad, M. Langseth, On the influence of constitutive relations in projectile impact of steel plates, International Journal of Impact Engineering 34 (2007) 464-486, 2007.
[25] X. Tenf, T. Wierzbicki, Evaluation of six fracture models in high velocity perforation, Engineering Fracture Mechanicals 73 (2006) 1653-1678, USA, 2006.
[26] T.J. Holmquist, G.R. Johnson, Determination of constants and comparison of results for various constitutive modes, Journal de Physique 4, Colloque C3, 1991.
[27] M. Asad, F. Girardian, T. Mabrouki, J.F. Rigal, Dry cutting study of an aluminum alloy (A2024-T351): a numerical and experimental approach, LaMCoS, CNRS UMR5359, France, 2008.
[28] J. Gardstan, Simulation of mechanical joining for automotive applications, Licentiate thesis from RIT, Departament of Mechanics, Sweden, 2006.

7. Symbols and Abbreviations

ε - Equivalent Plastic Strain
ε' - Plastic Strain Rate
ε'_0 - Reference Strain Rate (1.0 s^{-1})
ε'_{0f} - Plastic Strain at Damage Initiation
σ - Equivalent Plastic Flow Stress
σ_v - Yield Strength
σ_u - Ultimate Strength
ω – Johnson-Cook Scalar Damage Parameter
E - Elastic Modulus
ν - Poisson's Ratio
AZ – Anchoring Zone
BM – Base Material
CAD – Computer Aided Design
CAE - Computer Aided Engineering
E-P – Elastic-Plastic Model
FEM – Finite Element Method
HV - Vickers Microhardness
J-C – Johnson-Cook Criteria
PEI - Polyetherimide
PHAZ – Polymer Heat Affected Zone
PTMAZ – Polymer Thermo-Mechanical Affected Zone
MHAZ – Metal Heat Affected Zone
MTMAZ – Metal Thermo-Mechanical Affected Zone
S – Stress
U – Displacement